FIRST Telescope

Optical and Optomechanical Report

September 1999

Compiled by

Anthony B. Hull
Jet Propulsion Laboratory

19 September 1999

1. INTRODUCTION

1.1 Objective and scope

The Optical and Optomechanical Report is an evolving document, which shall be revised and expanded, and ultimately will constitute a comprehensive discussion of all optomechanical design parameters relevant to systems analysis and instrument development. Specifically excluded from this report are detailed discussions of the internal architecture and manufacturing processes of the primary mirror M1, of development of thin film coatings for emittance and reflectance control, and of the manufacturing and test processes for the rest of the telescope and its breadboard constructions. Although such data may influence the telescope opto-mechanical design characteristics, the details of these will be discussed elsewhere. However, the interpretation of these influences will underlie many of the analyses presented in the ultimate version this report, and will be summarized there.

The data presented in this report is the best current representation of our design, but is not a final definition of these aspects of the telescope. In the chapters submitted, some values or chapter sections remain 'To Be Done', and as such, are designated TBD. In other instances, representative parameters are tabulated and analyzed, but further constraints may evolve in the detailed design and optimization process, and these parameters may be changed.

These chapters shall ultimately represent the extent of compliance to FIRST Telescope Specification PT-RQ-04671, and also provide information required by the spacecraft and instrument designers for systems studies. Design margins will provide a basis for formal risk analysis, and system trades and optimizations. Results shall comprise the basis for internal specifications of telescope parameters that may either supplement, or more tightly constrain, those in PT-RQ-04671.

1.2 Contents

This September 1999 submission includes preliminary versions of two chapters: TELESCOPE OPTICAL DESIGN and MECHANICAL DESIGN OF TRIPOD LEGS. Substantial work has been done on other areas of design, and early versions of further chapters shall be submitted in the near future.

The Optical and Optomechanical Report shall include the following chapters:

1) Introduction
2) Telescope Description and Interface Compliance
3) Telescope Optical Design
4) Stray Light Analysis and Control
5) Mechanical Design (Presently just of the tripod legs)
6) Alignment Strategies and Error Allocations Derived from Performance Sensitivities to Environmental Perturbations, and Predicted Dimensional Stability and Control
7) Standing Wave Study, and Impact on the Telescope Design

1.3 Alignment Control

Alignment control shall be covered in depth in Chapter 6. Since this Chapter is not presented at this time, the process of establishing the requirements is outlined in the following. While low expansion materials of established temporal and thermal stability are used throughout, and while the specified alignment vectors allow latitude, the unusual speed of the telescope, and its high magnification, are recognized. Accordingly, the sensitivity of optical performance to alignment perturbations may be high. These perturbations include the classical parameters of despace, decenter and tilt of both the primary reflector M1 and the secondary reflector M2, and any changes in the radius of curvature (ROC) of either M1 or M2. Historical and empirical materials studies, together with expected mechanical tolerances, shall be used to estimate the statistical expected performance of each metering element of the telescope.

Since the telescope is tested at 1-g, and in a simulated thermal environment, certain errors will be present that are not fully representative of the telescope in service. The test environments provide additional constraints on thermal-mechanical design. Furthermore, the testing of telescopes of the size of FIRST present challenges and uncertainties.

Perturbations will be combined with optical sensitivities (to be provided in Chapter 3) plus estimated metrology and environment uncertainties to yield expected optical performance. An iterative process will be used to establish internal tolerances for all parts of the system. The degree that perturbations can be understood or controlled through launch, and at the L2 environment, shall be evaluated. A possible outcome of this analysis is that actuation of M2 with respect to M1 may be indicated. Such an indication would be manifestation of a significant probability that the performance would fall outside of required values, and could be improved by actuation, or that the performance could be significantly improved by actuated peaking.

Indication of actuation, if any, may involve 1, 3 or 5 degrees of freedom. The complexity of actuation increases with the number of degrees of freedom, and it is recognized that even a single actuator introduces both a risk element (probability of failure and consequence of failure), and a complexity at both the telescope and spacecraft level. The results of the perturbation-sensitivity analysis mentioned above should speak for themselves. At that time, the cost, complexity and risk of including actuation can be balanced against the risk and potential utility loss of not actuating. Due to the limited volume for actuation behind M2, compact non-orthogonal actuation strategy is likely to be adopted should actuation be needed.

1.4 Optical Error Correction

Control of fabrication and environmental response errors in M1 is potentially the greatest challenge in producing the FIRST telescope. Fortunately, not all system wavefront errors need to be controlled at M1. Chapter 3 shall include discussion of evaluations of the extent that M1 surface errors of various correlation lengths and amplitudes can be corrected for the system at M2. M2 is envisioned to be a modestly lightweighted stable

component in the optical system. With a glass ceramic substrate (currently Zerodur is planned), the mirror can easily be finished to visible imaging quality using computer controlled finishing machines, and tested at 633nm using a HeNe interferometer and (large) Hindle Sphere. Unambiguous mid-frequency and low frequency surface quality data will be available, and can be combined with M1 error maps to establish the degree that M1 errors are nullified by figuring M2. Thus, first room temperature distortions, and then cryogenic distortions, can be addressed by optically finishing M2, which is only a little over 300 mm in diameter, rather than M1 which is much larger.

1.5 Contributors

The main author of Chapter 3 is Don Small of LWO, and of Chapter 5 is Javier Escobedo of COI. Eri Cohen has reviewed early versions of these manuscripts and made useful comments, and others at LWO, COI and JPL have made contributions.

3. TELESCOPE OPTICAL DESIGN

3.1 Optical Design

3.1.1 Discussion

The baseline optical design for the (FIRST) is a Ritchey-Chretien design. This is one of two basic two-mirror telescope designs used for astronomical applications. The other design, the Cassegrain, consists of a parabolic primary mirror and a hyperbolic secondary mirror. This design produces perfect images on axis but suffers from the third order aberrations of coma, astigmatism, and field curvature at points off the optical axis. The performance of the system can be improved by making the primary slightly hyperbolic and compensating for this change by increasing the eccentricity of the secondary to produce a perfect image on axis. With the proper choice of eccentricities for the primary and secondary, both the spherical aberration and the coma can be corrected, leaving astigmatism and field curvature uncorrected. This system is called a Ritchey-Chretien (RC) system.

The baseline optical design for the Far Infrared Space Telescope is an F/8.68 Ritchey-Chretien (RC) design with an EFL of 28.50m yielding an effective aperture diameter of 3283 mm. The design is almost completely determined by the specification (FIRST Telescope Specification PT-RQ-04671). The primary and secondary radii and the primary to secondary spacing can all be derived from the specification. The only undetermined values are for the conic constants ($-e^2$) of the primary and secondary mirrors and the shape of the best-fit focal surface. The conic constants of the primary and secondary were chosen to result in an RC design rather than a Cassegrain design because the reduced coma at off-axis field points significantly reduces the telescope sensitivities to mirror tilts and decenters.

The telescope consists of a large primary mirror and a relatively small secondary. The primary mirror diameter is 3500 mm with a vertex radius of 3500 mm, a conic constant of –1.00129, and a focal length of 1750 mm. In order to improve the stiffness of the primary, the thickness has been increased from 125 mm to 203.2 mm. This increase in thickness was achieved without changing either the effective aperture, or the F/#. It was necessary to increase the specified distance from the primary mirror vertex to (1) the fixation plane location (where, according to TEFU-010, the telescope interfaces mechanically with the PLM interface structure via 3 hard points) and to (2) the best on-axis focus location (t_b in TEPE-030 and t_v in TEPE-035 respectively).

The secondary is held in place by three struts that run from the back of the secondary and attach through radially compliant flexures to mounts within the body of the primary mirror. The secondary mirror has a diameter of 308 mm, a vertex radius of curvature of 345 mm, and a conic constant of –1.29600. Because the aperture stop is located at the secondary mirror, the footprint of the entering beam at the primary mirror is a function of field angle. To prevent vignetting at the primary mirror, the diameter of the mirror must be greater than 3466 mm. The primary mirror diameter of 3500 mm allows for reduced surface accuracy near the edge of the mirror and reduces the effects of diffraction from the edge of the primary mirror

3.1.2 Optical Design Diagram and Notation

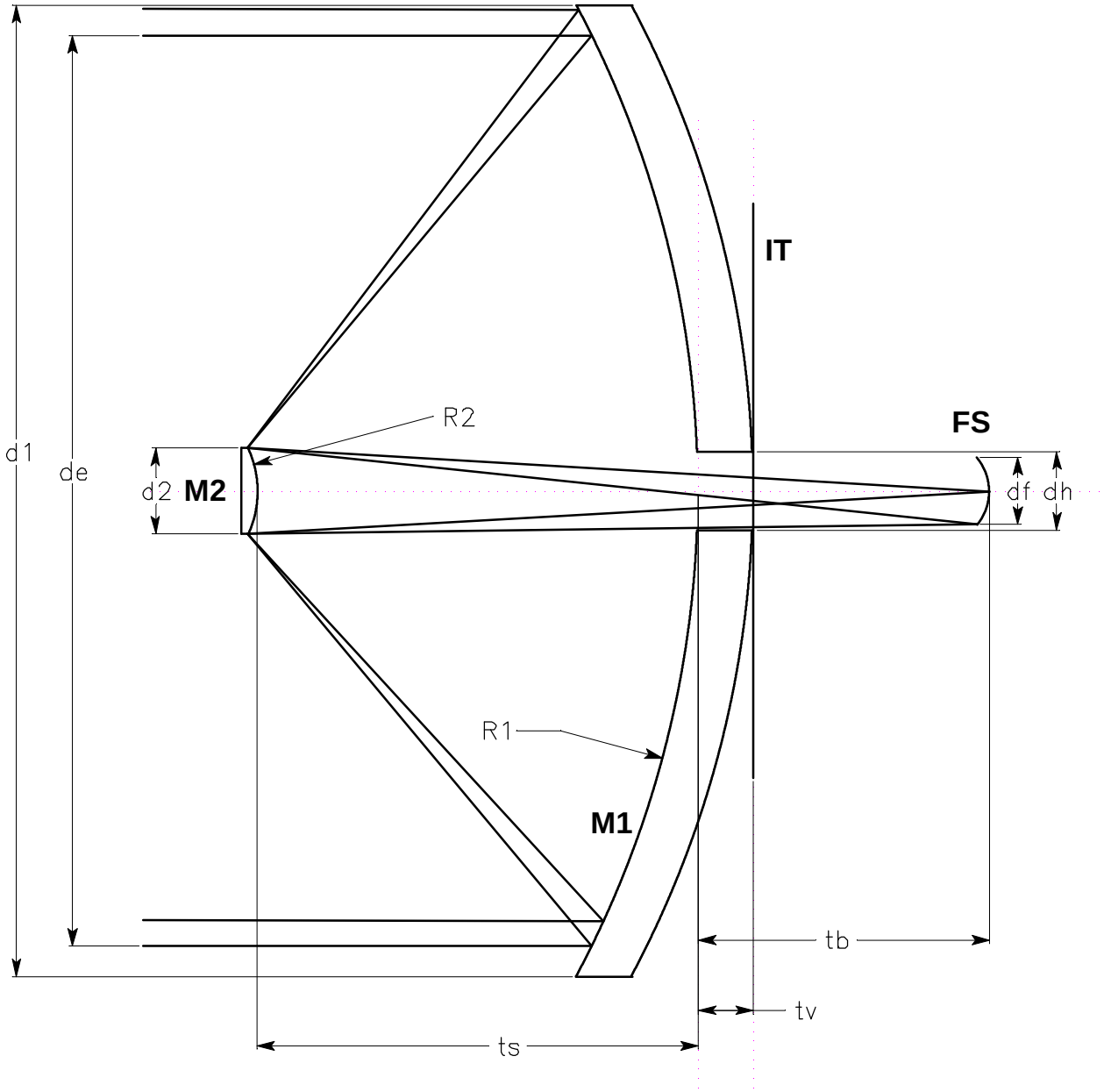

Figure 5.1 **NOT TO SCALE** Schematic of the telescope showing ray paths at 0 and -0.25º: M1, primary mirror; M2, secondary mirror; FS, focal surface; d1, primary mirror diameter; de, effective aperture diameter; d2, secondary mirror diameter; df, diameter of focal surface; dh, diameter of central hole in primary mirror; R1, vertex radius of curvature of primary mirror; R2, vertex radius of secondary; t_s, primary to secondary vertex distance; t_v, primary vertex to interface triangle; t_b, primary vertex to best axial focus location. Note that dh is to be established by stray light arguments, and is not yet known.

3.1.3 FOV Diagram Showing Placement of the Instruments (To Be Done (TBD))

3.1.4 Compliance

The compliance table below lists some of the specification requirements and the design values associated with the baseline optical design.

Number	Requirement	Value	Design
TEPE-015	Primary diameter	3500+2/-0 mm	3500 mm
TEPE-020	Primary F/#	0.5	0.5
TEPE-030	Primary vertex to best focus	975 mm	1050.16 mm [a]
TEPE-035	Primary vertex to fixation plane	125 mm	200.16 mm [b]
TEPE-045	Operating wavelength range	80-670 μm	
TEPE-050	Wavefront error budget (rms)	≤10 μm, ≤6 μm goal [c]	≤ 2 μm [d]
TEPE-065	Aperture stop location	secondary	secondary
TEPE-070	System focal length	28.50 m+/-0.05m	28.50 m
TEPE-075	Field-of-view	+/- 0.25º	+/- 0.25º

a. Primary to best focus distance increased by 75.16 mm to accommodate thicker primary mirror. Mirror thickness increased to meet stiffness requirements.
b. Primary vertex to fixation plane distance increased to accommodate thicker primary mirror.
c. To fully achieve its goals, the HiFi instrument requires that the goal be achieved.
d. The design Wavefront error is at edge of the field, and applies before manufacturing, alignment or environmental errors are considered

Table 5.1

3.2 Optical Design

3.2.1 Prescription

The optical design being presented is a baseline design; it is not the final design. The design was fixed at this point so that we would all have the same design to talk about. The design is close enough to the final design to use for tolerancing, and close enough to use for instrument design. The optical prescription below lists details of the baseline design. There appear to be some discrepancies in the listing. That is because some of the calculations are based on real ray data and some are first order calculations and in some cases because the calculations were only carried out to 5 places by the designer. For instance, the working F/# of the system is 8.680085 because the designer rounded the aperture stop radius to 154.15 rather than a more accurate value of 154.151510 (to the nearest nanometer). The errors in the design are much smaller than the expected fabrication and alignment errors and thus may be ignored. For instance, to change the effective focal length (efl) of the system from 28499.722 to exactly 28500 mm would require a change in the primary to secondary spacing of 0.103 μm.

System/Prescription Data

Surfaces: 2
Stop: 2 (aperture stop located at secondary mirror surface)
System Aperture Stop Radius: 154.15 mm (radius) equals the radius of M2
Eff. Focal Len: 28499.72 mm (in image space)
Back Focal Len: 2638.131 mm (Axial distance from secondary to image surface)
Working F/#: 8.680085 mm (based on a real-ray trace)

Effective Aperture Dia. 3283 mm (EFL/Working F/# following from TEPE-070)
Exit Pupil Dia.: 308.3 mm (Same as secondary diameter)
Exit Pupil Pos.: -2638.131 mm (Exit pupil distance from focal surface)
Maximum Field: 0.25 degrees
Primary Wave: 1 micrometer (Used so wavefront error is in micrometers)
Lens Units: millimeters

SURFACE DATA SUMMARY:

Surf	Comment	Radius	Thickness	Glass	Diameter	Conic
OBJ	Object	Infinity	Infinity			
1	Primary mirror	-3500	-1587.969	MIRROR	3465.361	-1.00129
STO	Secondary Mirror and Aperture Stop	-345.264	2638.131	MIRROR	308.3000	-1.29600
IMA	Focal Surface	-167.171			244.9497	-1

Optical Curvature Depth $|\Delta x|$ for M1, M2 and IMA

M1	437.465mm over 3500mm diameter
M2	33.919mm over 308.3mm diameter
IMA	44.865mm over 244.9497mm diameter

Design Performance

3.2.1.1 Design Wavefront Error

The Wavefront error of the baseline optical design is listed below. The Peak to Valley (P-V) wavefront error is the difference between the highest and lowest points in the wavefront. Both the RMS and P-V wavefront errors are relative to a parabolic focal surface.

Wavefront error

Field angle, arcminutes	P-V μm	RMS μm
0.0	.26	.07
10.5	6.63	.96
15.0	10.90	1.93

The plots below show the wavefront error for field angles of 0.000, 0.175, and 0.250 degrees. The plot are all to the same scale for ease of comparison.

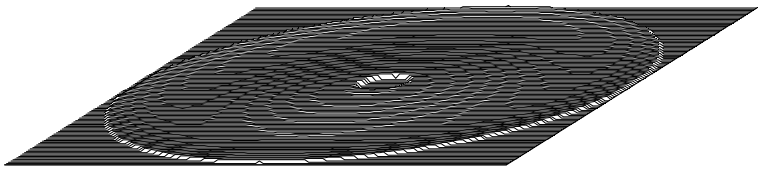

Wavefront Error On-axis (0.26 λ P-V)

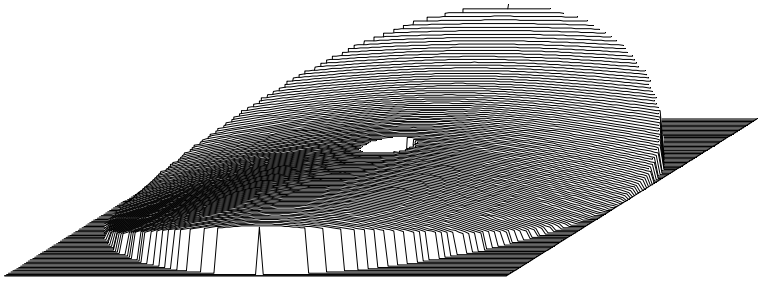

Wavefront error at 0.7 field (6.63 λ P-V)

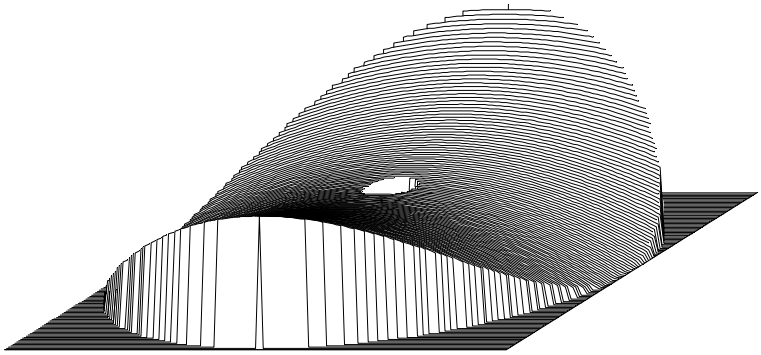

Wavefront error at 1.0 field (10.90 λ P-V)

3.2.1.2 Point Spread Functions

The point spread functions shown below are calculated at the shortest wavelength, where system aberrations would cause the most degradation. At this wavelength the PSFs are almost indistinguishable. The Strehl ratio is the ratio of the height of the PSF of an aberrated system to that of a perfect system. The Strehl ratios in the table below show that even at the shortest wavelength there is very little image degradation.

Design PSF

Field angle, arcminutes	Strehl Ratio @ 85 μm
0.0	1.00
10.5	.995
15.0	.981

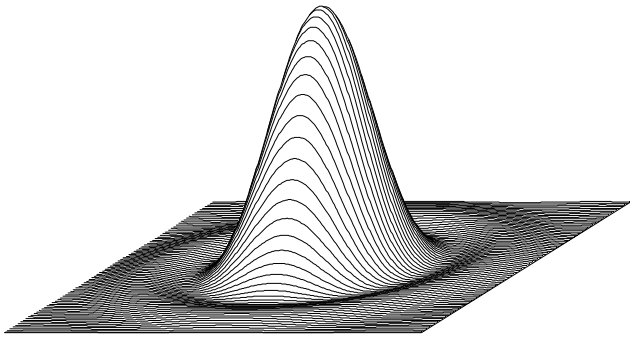

PSF On-axis at 85μm (1.00 Strehl ratio)

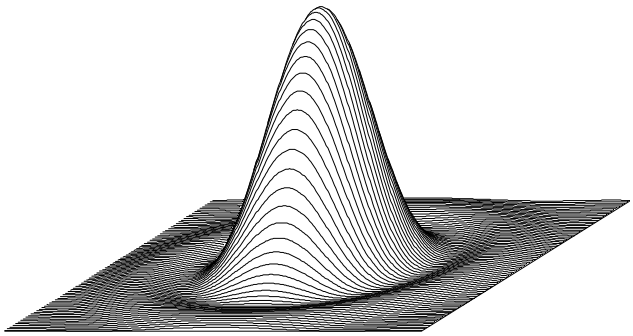

PSF 0.7 field at 85μm (0.995 Strehl ratio)

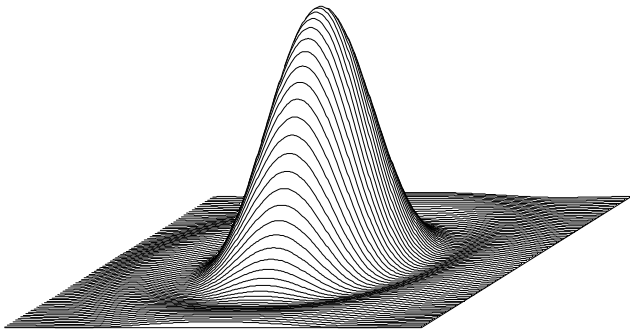

PSF 1.0 field at 85μm (0.981 Strehl ratio)

3.2.1.3 Focal Plane, Curvature, Astigmatism, and Distortion

The focal surface is highly curved. The best focus (from a flat focal plane) at the edge of the field is –47.49 mm for tangential rays and –41.94 mm for the sagittal rays. The plots below show the field curvature and distortion relative to the baseline parabolic focal surface and relative to a flat focal plane. Note that the curved focal surface fits the best average surface very well. Also note that the distortion is significantly increased on the curved focal surface.

Field Curvature Distortion

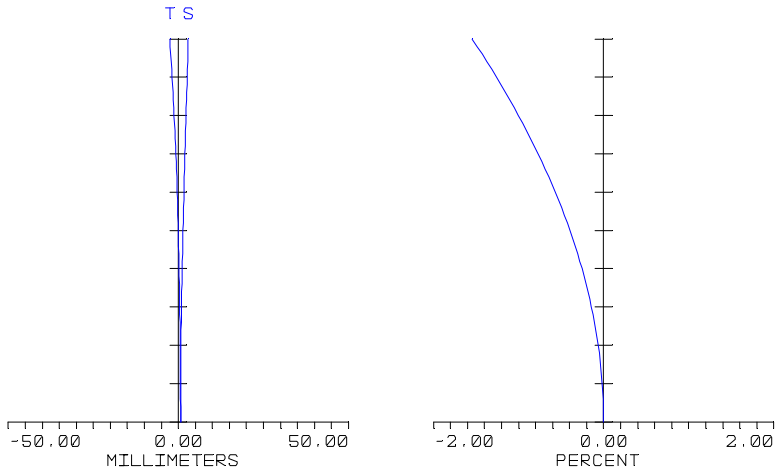

Tangential and sagittal focal surfaces and distortion for parabolic focal surface. The ordinate ranges from 0% to 100% of field.

Field Curvature Distortion

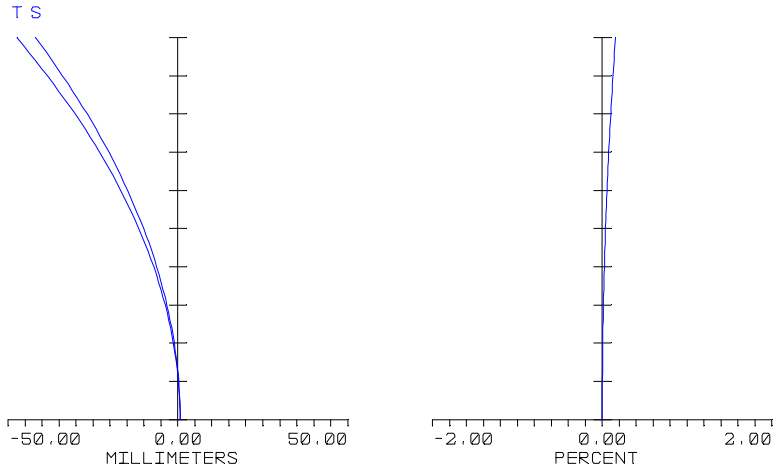

Tangential and sagittal focal surfaces and distortion for flat focal surface. The ordinate ranges from 0% to 100% of field.

3.2.2 M1 error correction on M2 (TBD)

3.2.2.1 Effective Aperture on M1

The instantaneous aperture at M1 is 3280 mm; this is the diameter of the bundle of rays at the primary that will just fill the secondary. Because the instantaneous aperture moves around on the primary as a function of field angle, the area of the primary that is used is larger than the instantaneous aperture. The minimum clear aperture required for zero vignetting over the full 0.5 degree field is 3466 mm

3.2.2.2 M1 Minimum and Maximum Hole Diameter

3.2.2.2.1 **The minimum hole diameter** in the primary optical surface required to clear all rays is 269 mm. This is the diameter required to clear all rays at the maximum field angle of 0.25 degrees.

3.2.2.2.2 **The maximum hole diameter** allowable that does not vignette any rays [rays that are not obscured by the secondary] in the full +/-0.25 degree field is 294 mm. This is the maximum diameter the hole can be without allowing some rays within the field-of-view to pass directly through the hole in the primary to the focal surface.

3.2.2.3 M2 Properties

3.2.2.3.1 The **primary to secondary spacing** is 1587.97 mm. This distance can be calculated from the focal length of the primary, the focal length of the system, and the primary vertex to best focus distance.

3.2.2.3.2 The **secondary magnification** is 16.286 = (system focal length) / (primary focal length).

3.2.2.3.3 The **secondary diameter** is 308.3 mm. A first order approximation can be calculated from the back focal length and the system F/#. Secondary diameter ≅ (BFL) / (F/#) = 2638.13 / 8.68 = 303.93mm. This does not take into account the sag of the secondary which, of course, is not known until the diameter is known.

3.2.2.3.4 The **central 13.34 mm of the secondary mirror is not illuminated** by any rays within the field-of-view of the telescope. This portion of the mirror could be removed with any loss in illumination of the focal surface. No light strikes this area because it is in the shadow of the secondary mirror itself. As light enters the telescope, some of it is blocked by the secondary mirror. The blocked light produces a shadow on the primary mirror. This shadow is reflected to the secondary mirror. From any given field point the shadow of the secondary on the secondary forms a nearly circular disk 28.56 mm in diameter. At field angles other than zero the shadow is displaced from the center of the mirror. At 0.25 degrees field the shadow is displaced about 7.6 mm. It still covers the center of the mirror but at radial distances between 6.67 and 21.87 mm only part of the mirror is in shadow. At different field positions the secondary shadow falls at different locations on the secondary. However, there is an area with a radius of 6.67 mm that is always in the shadow.

3.3 Sensitivities
3.3.1 Sensitivity Diagram

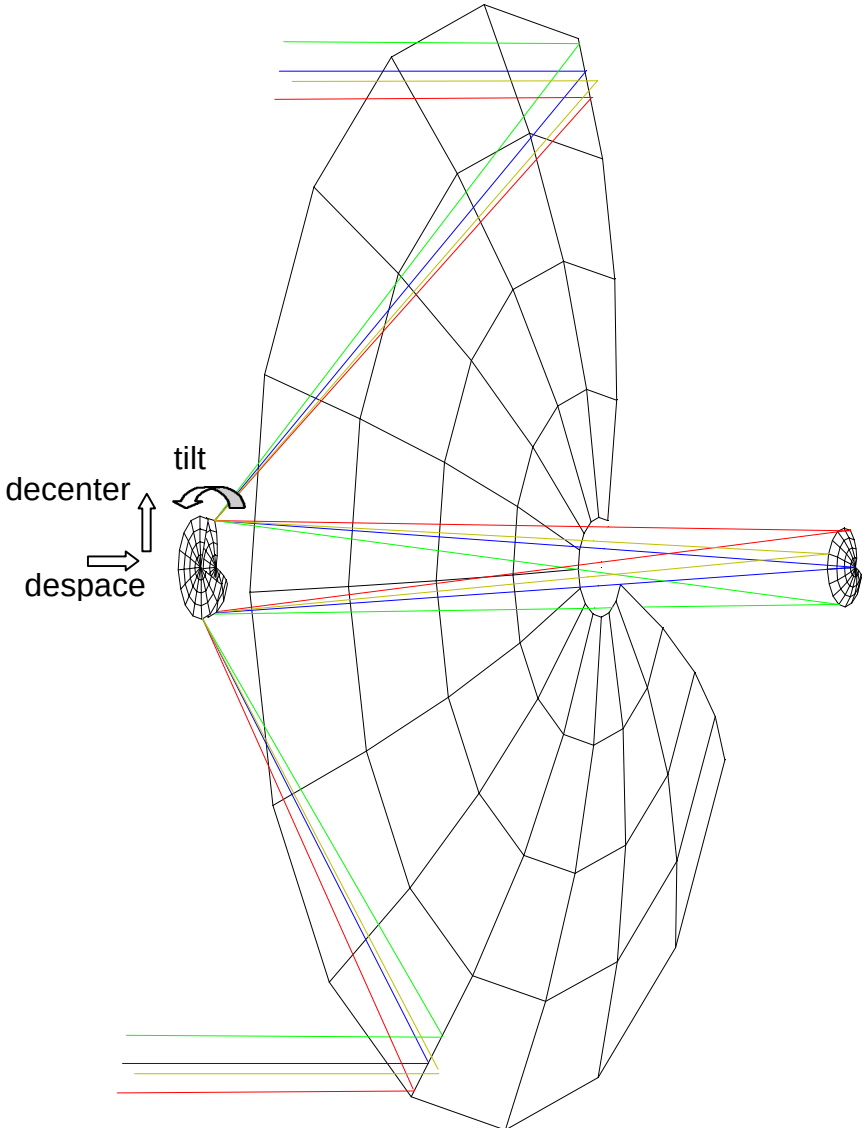

Diagram showing despace, decenter, and tilt of secondary.

Table of Sensitivities $\partial W_j/\partial x_i$ (TBD)

3.3.2 Relate to alignment vector (TBD)

3.3.3 Boresight diagram and sensitivity (TBD)

3.4 Test (TBD)

3.4.1 1-g error discussion (TBD)

3.4.2 Vertical test (TBD)

Appendix

System/Prescription Data (ZEMAX Form)

LENS NOTES:

F/8.68 using real rays parabolic focal plane

GENERAL LENS DATA:

Surfaces: 5
Stop: 3
System Aperture: Float By Stop Size = 154.15
Glass Catalogs: Schott
Ray aiming: Real Reference, cache on
X Pupil shift: 0
Y Pupil shift: 0
Z Pupil shift: 0
Apodization: Uniform, factor = 0.00000E+000
Eff. Focal Len. : 28499.72
Eff. Focal Len. : 28499.72 (in image space)
Back Focal Len. : 2638.772
Total Track: 2700.162
Image Space F/#: 8.559106
Para. Wrkng F/#: 8.559106
Working F/#: 8.680085
Image Space N.A.: 0.0583179
Obj. Space N.A.: 1.664874e-007
Stop Radius: 154.15
Parax. Ima. Hgt.: 124.3543
Parax. Mag. : 0
Entr. Pup. Dia. 3329.755
Entr. Pup. Pos.: 18800.65
Exit Pupil Dia.: 308.3
Exit Pupil Pos.: -2638.131
Field Type: Angle in degrees
Maximum Field: 0.25
Primary Wave: 1
Lens Units: Millimeters
Angular Mag. : 10.80037

Fields: 3
Field Type: Angle in degrees

#	X-Value	Y-Value	Weight
1	0.000000	0.000000	1.000000

2	0.000000	0.175000	1.000000
3	0.000000	0.250000	1.000000

Vignetting Factors

#	VDX	VDY	VCX	VCY
1	0.000000	0.000000	0.000000	0.000000
2	0.000000	0.000000	0.000000	0.000000
3	0.000000	0.000000	0.000000	0.000000

Wavelengths : 1
Units: Microns

#	Value	Weight
1	1.000000	1.000000

SURFACE DATA SUMMARY:

Surf	Type	Comment	Radius	Thickness	Glass	Diameter	Conic
OBJ	STANDARD		Infinity	Infinity		0.00000	0.00000
1	STANDARD		Infinity	1650.000		3476.018	0.00000
2	STANDARD		-3500.000	-1587.970	MIRROR	3465.361	-1.00129
STO	STANDARD		-345.264	1587.969	MIRROR	308.300	-1.29600
4	STANDARD		Infinity	1050.162		268.8173	0.00000
IMA	STANDARD		-167.171			244.9497	-1.00000

SURFACE DATA DETAIL:

Surface OBJ : STANDARD
Surface 1 : STANDARD
Aperture : Circular Obscuration
Minimum Radius : 0
Maximum Radius : 160
Surface 2 : STANDARD
Aperture : Circular Aperture
Minimum Radius : 0
Maximum Radius : 1750
Surface STO : STANDARD
Surface 4 : STANDARD
Surface IMA : STANDARD

5. MECHANICAL DESIGN OF TRIPOD LEGS

5.1 General Description and Assumptions

The configuration currently being considered for the FIRST Telescope assembly consists of an all-composite primary mirror, a lightweighted Zerodur secondary mirror and its support structure, and composite tripod legs used to support the secondary reflector and its support structure.

The secondary reflector (M2) subassembly is supported by tripod legs that mount directly to the primary mirror (M1). The tripod legs are connected at the primary mirror, using the same fittings that connect the primary mirror to the triangular interface structure through flexures. Due to the location of the telescope fixation points, and the desire to keep as much as possible a direct load path between the fixation points and the tripod legs, the tripod legs pass through the primary mirror at a specific percentage of the aperture radius.

The tripod leg configuration must meet several mechanical requirements including deflections due to gravity, natural frequencies, and survivability requirements. In addition, the mechanical design must be compatible with the optical performance of the telescope system. In particular, obscuration and stray-light issues must be accounted for in the selection of the tripod configuration.

5.1.1 Mechanical System Requirements

The tripod legs must be designed such that the mechanical system requirements are met without affecting the optical performance of the telescope. The mechanical system requirements from the FIRST Telescope Specification used in the sizing of the tripod legs are the eigenfrequency requirements. The longitudinal eigenfrequency must be greater than 60 Hz (TEEN-110) and the lateral eigenfrequency must be greater than 45 Hz (TEEN-115). The torsional mode associated with the tripod legs must be greater than 31 Hz (ESA Response to JPL Questionnaire, PT-06827). Table 5.1 summarizes the frequency requirements associated with the tripod legs.

Requirement Code	Description	Requirement Value
TEEN-110	Longitudinal Eigenfrequency	> 60 Hz
TEEN-115	Lateral Eigenfrequency	> 45 Hz
in PT-06827 Memo	Torsional Eigenfrequency	> 31 Hz

TABLE 5.1 Stiffness requirements used to obtain tripod leg configuration

In addition to the eigenfrequency requirements, other stiffness requirements are imposed on the system to maintain the secondary mirror decenter, despace, and tilt at acceptable levels during testing under 1-g loading, depending on the testing configuration and

strategy. These additional stiffness requirements are considered internal to the design, and are not part of the Telescope Specification.

The design of the tripod legs is driven by the stiffness considerations, and other mechanical system requirements such as strength, fatigue, thermal, and moisture issues will be verified as the design becomes more refined.

5.1.2 Tripod Leg Current Structural Configuration

For structural performance purposes, the baseline tripod leg configuration can be selected by defining the material used, the cross-sectional properties, dimensions, and locations relative to the primary and secondary mirrors. The baseline configuration must be selected to meet the structural as well as optical requirements of the telescope. The current configuration considered in this study may need to be modified, or refined, in the future when a more detailed analysis of the components is performed. In the current configuration it was assumed that the mass supported by the tripod legs, which includes the secondary mirror and its support structure, is 4.54 kg. Since the detailed design of the secondary mirror support structure has not been completed at this time, it is necessary to investigate the structural behavior for a range of possible configurations with different masses. The analysis was repeated for several mass values, specifically at 2.27 kg, 3.4 kg, 4.54 kg, 5.67 kg, and 6.8 kg.

Figure 5.1 shows the tripod legs, primary mirror, and secondary mirror locations which are considered as the current configuration. Dimensions will be finalized when the detailed design, meeting the structural, environmental, and optical requirements, is completed.

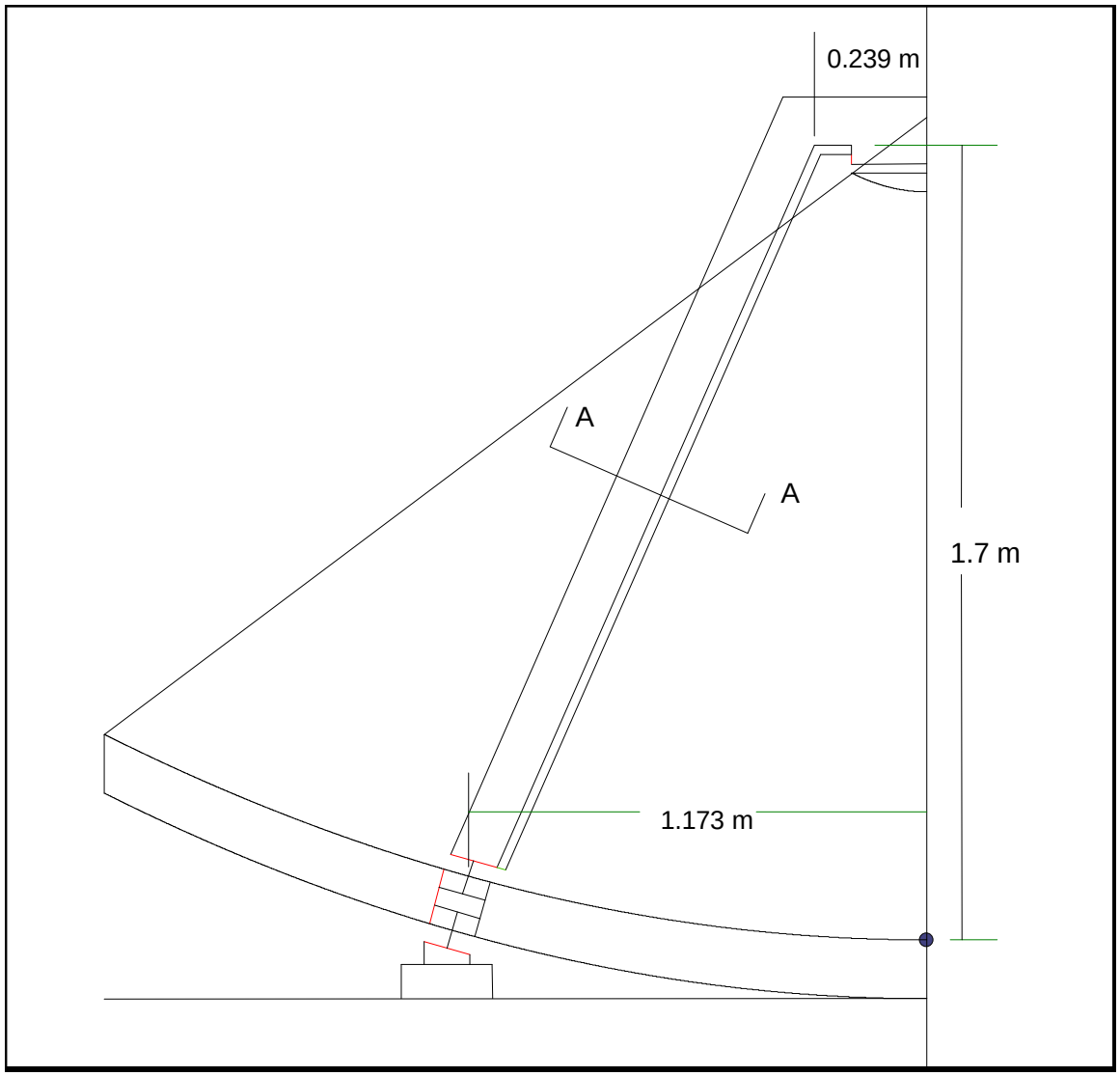

FIGURE 5.1 Preliminary telescope geometry showing tripod leg constraint location at sixty-seven percent of M1 aperture

Some parameters have been selected for the current configuration, even though they may differ from FIRST Telescope Specification values. For example, Figure 5.1 shows the tripod leg's position (center line) relative to the primary mirror front surface at 1.173 meters, which corresponds to sixty-seven percent of the aperture radius. Based on the concept shown in Figure 5.1, which has a direct load path between the tripod legs and the support structure, the triangular interface points would be at some small distance greater than 1.173 meters, which exceeds the 1.037 value (or fifty-nine percent) from the FIRST Telescope Specification. Design trade analyses covered the possible location of the tripod legs relative to the primary mirror aperture, corresponding to various constraint locations. The current configuration assumes that the ratio of the tripod leg constraint location to the aperture radius is sixty-seven percent since at this location the frequency requirements are met, obscuration is acceptable, and the location may provide an

optimum location for minimizing the primary mirror's deflection due to earth's gravity, without affecting the telescope's performance under operating conditions.

The top of the tripod legs are separated from the secondary mirror by a distance "e" (elbow separation) to decrease optical obscuration effects. For the purposes of the analysis, the elbow separation used is 239 mm. The structural performance of the telescope in greatly influenced by the height of the tripod legs. In Figure 5.1, the height of the tripod legs from the vertex of the primary mirror to the bottom of the tripod leg elbow is 1.7-meters. This dimension will be finalized as soon as the detailed design of the secondary mirror support structure is completed.

The increase in elbow separation would result in the top of one tripod leg being marginally illuminated by the sun, and accordingly, we are exploring chamfering of the tripod legs to prevent illumination. With our latest understanding of placement of the sunshield, precluding illumination will be more difficult than previously thought. Modifications currently being considered are secondary in terms of structural performance and are not considered in the structural analysis at this time. Modifications to the design, such as the chamfering of the top of the tripod legs, can be accomplished without affecting the structural response of the system.

In the configuration used in the analysis, the tripod legs have a rectangular cross-section which is constant throughout the length of the tripod legs. The cross section has a width of 19.05 mm, a depth of 102 mm, and a wall thickness of 1.02 mm. The tripod legs are arranged so that the width (the smaller dimension) corresponds to the circumferential direction of the mirror. A spoiler of depth equal to 19.05 mm is added to the tripod leg for optical considerations (i.e., stray light) and is not considered to be a structural component, although it is included in the mass budget. Figure 5.1 summarizes the geometry of the tripod leg cross section.

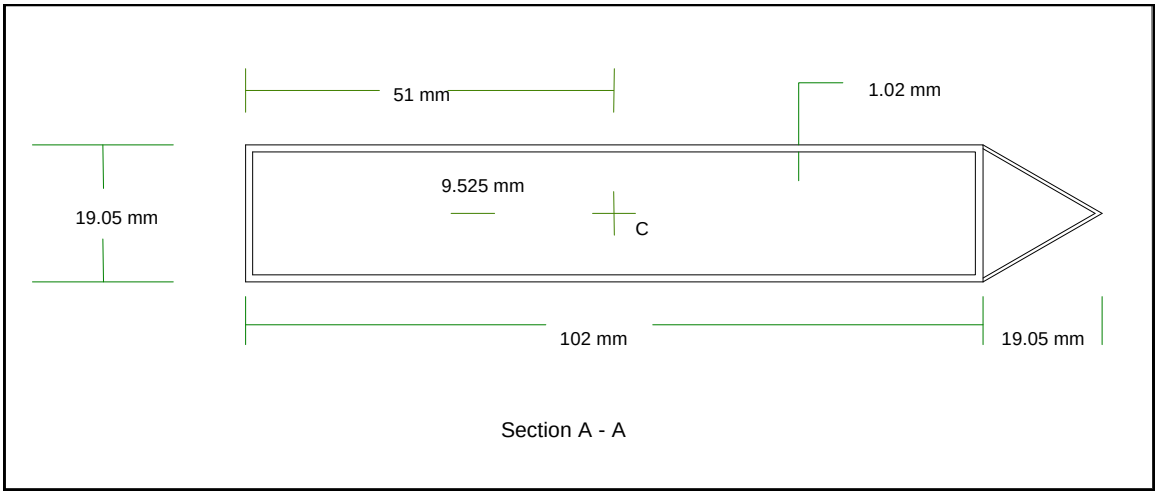

FIGURE 5.2 Tripod leg cross section geometry used in analysis

5.1.3 Material Selection

Due to the differences between optical and mechanical objectives, it is difficult to optimize simultaneously the optical and mechanical parameters defining the telescope. For example, the tripod legs should be as thin as possible in the circumferential direction to minimize obscuration, while stiffness requirements dictate that the cross-sections should be wider to increase the telescope eigenfrequencies and to minimize disturbances due to gravity during testing. A trade-off study is required to determine configurations which meet both sets of requirements. By properly selecting the materials, it is possible to improve the performance of a particular design without modifying the geometric parameters.. For these reasons, the material currently being considered for the tripod legs is a quasi-isotropic K13C2U/954-3 configuration (60% Fiber volume), which is much stiffer than the M55J/954-3 material used for the primary mirror. The values of the material properties of the tripod legs used in the analysis are summarized in Table 5.2.

	Modulus of Elasticity	Shear Modulus	Poisson's Ratio	Density
K13C2U/954-3 Quasi-Isotropic	177 GPa	67 Gpa	0.32	1800 kg/m^3

TABLE 5.2 Material properties used for the tripod legs in the analysis

Although the material configuration selected for the tripod legs is much stiffer than the material selected for the primary mirror, its density is also higher. This means that the performance improvements are more evident when considering deflections due to gravity than when considering eigenfrequencies.

Due to the differences in thermal expansion between the tripod leg material and the primary mirror material, the tripod legs will be tuned to match the thermal strain of the primary mirror by introducing a thermal expansion compensation scheme into the design. Since many material and layup configurations can be use to meet the desired structural objectives, the actual details of the configuration will be finalized when a design configuration which meets the specification requirements is selected.

5.1.4 Finite Element Modeling

Finite element analysis can used to select the initial geometry, and to demonstrate that structural requirements can be met. Selecting the initial geometry is necessary not only for structural purposes, but also to make stray light and obscuration predictions. These estimates are provided in other chapters of this report. Since the initial sizing requires a large number of analysis runs, several simplifying assumptions have been made in modeling the telescope assembly. Due to the simplifying assumptions, the results presented show that the requirements are achievable, but not necessarily that the selected geometries fully meet the specifications. The approximations used in the analysis include the following:

1) Each tripod leg is approximated as a set of 1-dimensional beam elements

2) The secondary mirror and support structure are approximated as solid Zerodur for stiffness, not mass
3) The connections between the tripod legs and the secondary mirror are assumed to be rigid, neglecting the connections flexibility
4) The primary mirror is modeled as a set of equivalent plates, representing axial, shear and bending behavior of the structure
5) The tripod leg to primary mirror connections for eigenfrequency computations were assumed to be constrained in the optical axis direction and in the tangential direction only, with all rotations and radial direction not constrained.
6) The tripod leg to primary mirror connections for deflection computations were assumed to be constrained from translating, but allowed to rotate freely.

These simplifying assumptions are reasonable for conducting the initial sizing of the telescope components. However, a more detailed analysis would be required to ensure that the specification requirements are met. The detailed analysis will be conducted after a baseline configuration that meets the structural, optical, and specification requirements is selected.

The structural performance of various tripod leg configurations was studied by modifying a simplified finite element model of the telescope. In the analysis, the tripod legs were modeled by using sixteen 1-dimensional beam elements along each tripod leg. Sixteen elements along the length of the tripod legs were selected to adequately capture the behavior in the analysis.

The secondary reflector subassembly was modeled using plate elements with very high stiffness properties (i.e., assuming that the stiffness is that of a massless, 2.54 cm monolithic Zerodur plate). The predicted mass of M2 and its support structure was uniformly distributed over the plate elements. The tripod legs were connected to the M2 subassembly plate elements by using rigid elements, allowing the tripod legs to be offset from the edge of the M2 subassembly. The offset was introduced to the design to reduce the obscuration due to the tripod leg configuration.

In order to model the stiffness of the primary mirror, the tripod legs were connected to an equivalent model of the primary mirror, which consists of plate elements with equivalent stiffness properties. The equivalent stiffness properties are approximations since the properties of the 3-dimensional, composite primary mirror are “smeared” over the set of plate elements. The bottom of each tripod leg was connected to several nodes in the primary mirror by using rigid elements. The primary mirror was then constrained by assuming a kinematic mount condition when computing eigenfrequencies. In this section, a kinematic mount means that for each of the constraint locations, one of the nodes at which the rigid elements were connected was constrained to prevent motion in the optical axis direction and in the tangential direction (θ-direction). The radial direction and the rotations were not constrained. Figure 5.3 shows the finite element model used in computing the eigenfrequencies and deflections of the telescope.

When computing the deflections due to gravity, the equivalent model of the primary mirror was omitted from the analysis, and the tripod leg bases were assumed to be pinned. For the purposes of this section, a pinned constraint means that the boundary conditions prevented any translation, but allowed the tripod leg bases to rotate freely. These assumptions were used to determine the deflections attributable to the tripod legs, and neglect the contribution of the flexures and support structure (which can be accounted for separately). Table 5.3 summarizes the assumptions and details of the finite element analysis computations.

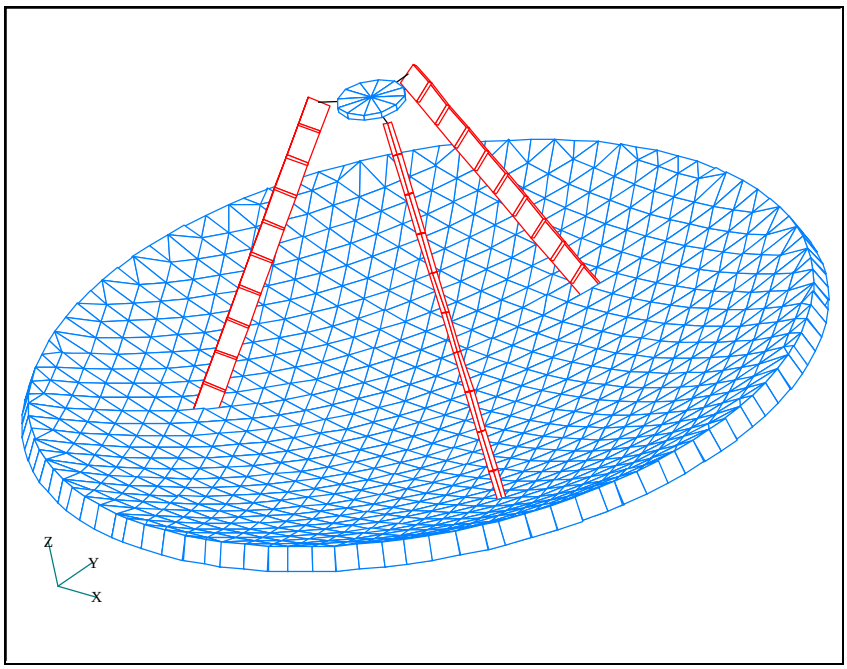

FIGURE 5.3 Finite Element Model Used for Sizing Tripod Legs: Beam and plate elements are displayed with their thicknesses shown

Finite element software	**MSC/NASTRAN Version 70.0.1**
Elements used for tripod legs	**16 beam (CBEAM) elements per leg**
Elements used for M2 and support	**12 plate (CTRIA3) elements**
Connection between M2 and tripod legs	**Rigid (RBE2) elements**
Elements used for primary mirror	**1518 plate (CTRIA3) elements**
Constraints for computation of eigenfrequencies	**kinematic mount:** **all rotations and radial displacement free; optical axis and tangential direction fixed**
Constraints for computation of deflections	**Pinned constraints:** **Constrained in all directions; Connections allowed to rotate freely**

TABLE 5.3 Assumptions used in finite element analysis computations

The modeling assumptions used for determining the tripod leg configuration are adequate for initial sizing and for preliminary assessment of the structural performance. The assumption that the secondary mirror subassembly is stiff was used since the design of the M2 subassembly has not yet been completed.

These assumptions may lead to higher frequencies than those which would be obtained with a more realistic model of the M2 support subassembly. However, the emphasis is in arriving to feasible configurations, and not necessarily in generating models with the necessary details to ensure that the specification requirements can be met. In order to account for the depths of various components (for example, the primary mirror depth), the tripod legs were assumed to be an additional 12.7 cm longer in the finite element models.

It should be understood that the finite element models are preliminary in nature, and that various details are not modeled, since the design of all the telescope components has not yet been completed. As mentioned above, the secondary mirror support subassembly has not been finalized. Also, details such as chamfering the tripod leg to prevent sun illumination are considered secondary in nature in terms of structural performance, and thus are not included in the preliminary analysis.

5.2 Analysis Under Launch Environment Conditions

5.2.1 Dynamic Analysis

Using the modeling assumptions described previously, a dynamic analysis was performed to determine the eigenfrequencies and mode shapes associated with the tripod legs. The computed eigenfrequencies are useful since they indicate possible resonance of the structure if excited at those frequencies. The mode shapes corresponding to the eigenfrequencies describe the expected deformation pattern of the structure if excited at those frequencies. The predicted eigenfrequencies are compared with the frequency requirements described in Section 5.1 to ensure that the design meets and exceeds the frequency requirements.

5.2.1.1 Dynamic Analysis Results of Current Configuration

The dynamic analysis results that follow correspond to a tripod leg configuration with the constraint location at sixty-six percent of the aperture radius, and a mass of 4.54 kg supported by the tripod legs. The location is at sixty-six percent, and not at sixty-seven percent, of the aperture simply because of the way the finite element model was generated. The sensitivity of the results, as parameters are allowed to change, are presented in the next section. The parameters used in the sensitivity study include the mass supported by the tripod legs (simulating the secondary mirror and its support structure), and the constraint location. For the purposes of this report, the constraint location means the location of the base of the tripod legs relative to the aperture of the primary mirror, given as a percentage value.

The fundamental vibration mode shape of the structure corresponds to torsion of the tripod legs about the optical axis. The corresponding predicted fundamental frequency is 43.0 Hz (31 Hz requirement) with a corresponding effective mass of 0.4 percent. The torsional mode shape is shown in Figure 5.4.

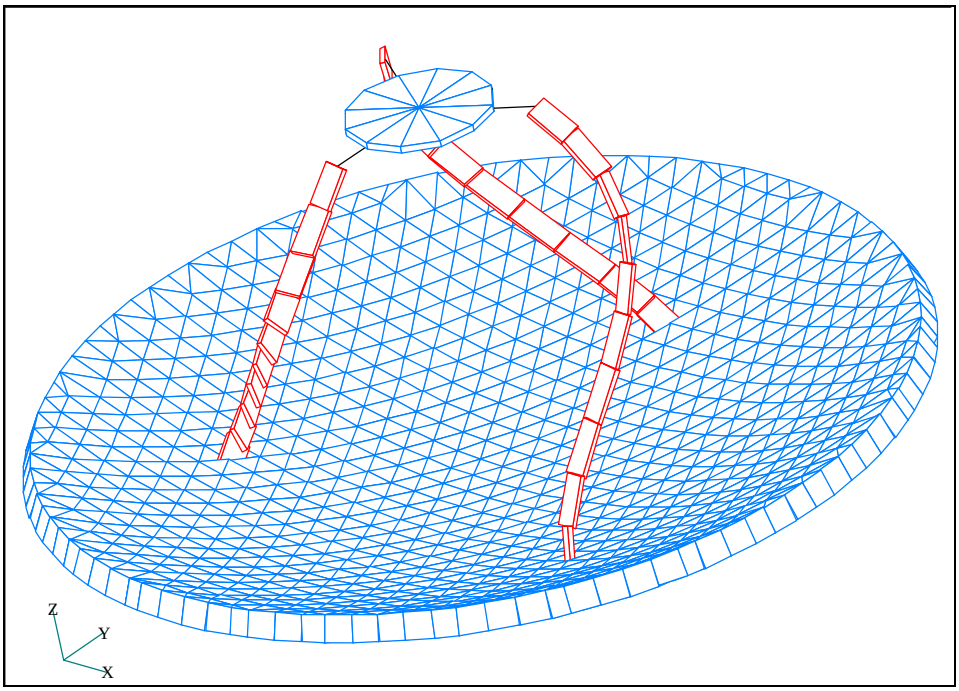

FIGURE 5.4 Torsional mode shape for case with constraint location at 66% of the aperture:
Legs supporting 4.54 kg; Eigenfrequency 43 Hz (requirement: > 31 Hz)

The first vibration mode shape in the transverse direction occurs at a frequency of 76.7 Hz (45 Hz requirement), with a corresponding effective mass of 6.1 percent. See Figure 5.5.

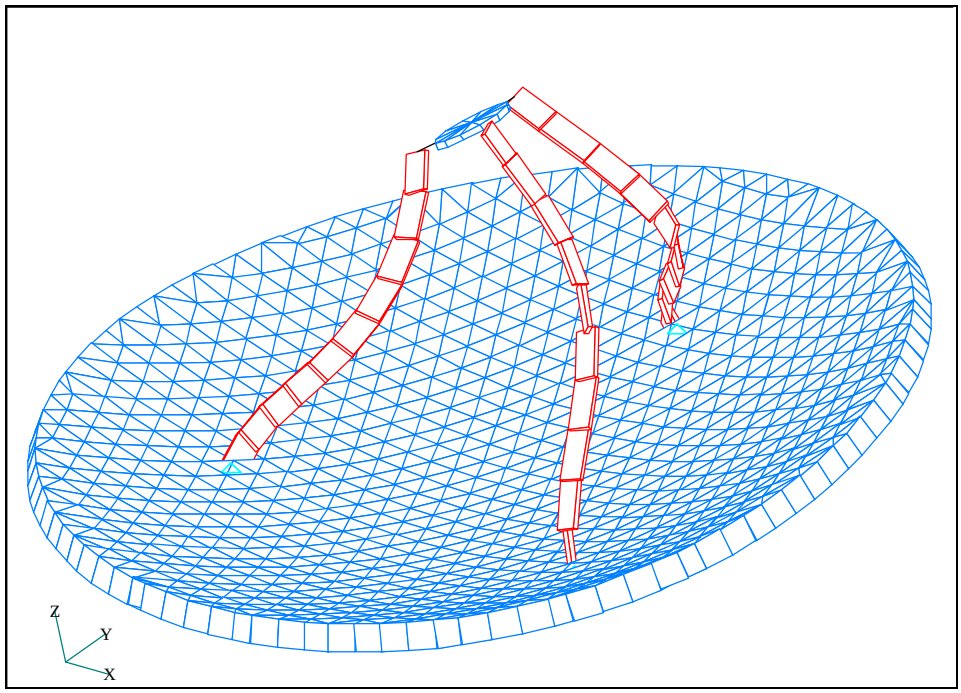

FIGURE 5.5 Transverse mode shape for case with constraint location at 66% of the aperture:
Legs supporting 4.54 kg; Eigenfrequency 76.7 Hz (requirement: > 45 Hz)

The first vibration mode shape in the longitudinal direction occurs at a frequency of 152 Hz (60 Hz requirement), with a corresponding effective mass of 52 percent. See Figure 5.6.

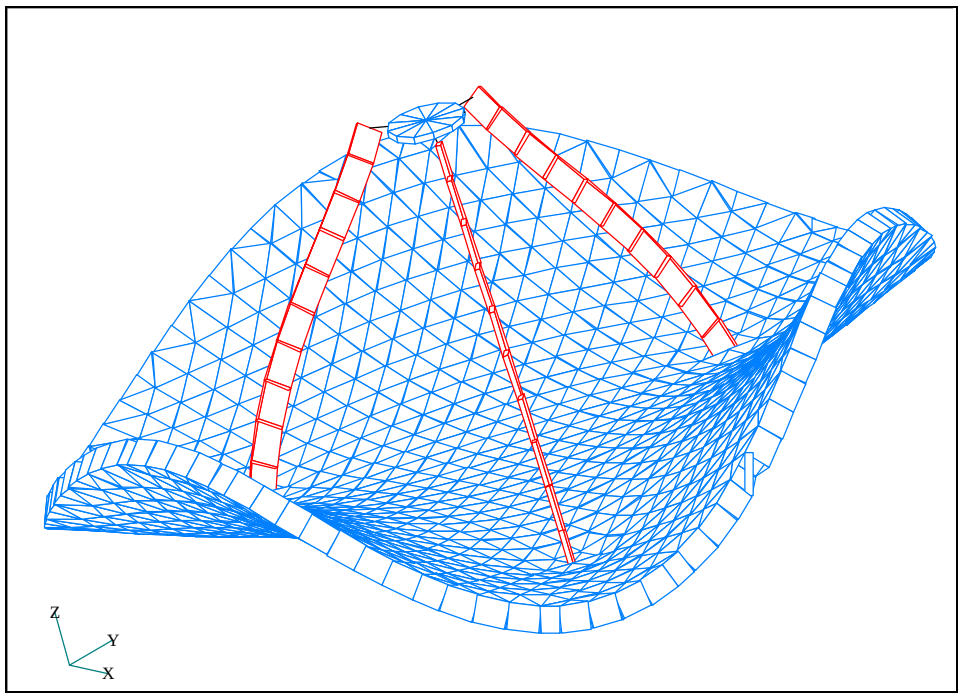

FIGURE 5.6 Longitudinal mode shape for case with constraint location at 66% of the aperture:
Legs supporting 4.54 kg; Eigenfrequency 152 Hz (requirement: > 60 Hz)

Table 5.4 summarizes the eigenfrequency results for the analysis configuration with the constraint location at sixty-six percent of the aperture.

Requirement Code	Description	Requirement	Values at 66% of aperture
TEEN-110	Longitudinal Eigenfrequency	> 60 Hz	152 Hz
TEEN-115	Lateral Eigenfrequency	> 45 Hz	76.7 Hz
in PT-06827 Memo	Torsional Eigenfrequency	> 31 Hz	43 Hz

TABLE 5.4 Material properties used for the tripod legs in the analysis

5.2.1.2 Sensitivity to Current Configuration Parameters

In order to ensure that the current tripod configuration is acceptable, the sensitivity of the dynamic performance was studied as a function of several tripod configuration parameters. In particular, the sensitivity to changing the mass supported by tripod legs, and to changing the constraint location was studied. The range of the mass supported by the tripod legs changed from 2.27 kg to 6.8 kg with 4.54 kg as the baseline. The constraint location ranged from 60% to 78% of the aperture radius.

The sensitivity of the torsional, transverse, and axial frequency as a function of supported mass and constraint location are shown in Figures 5.7 to 5.9.

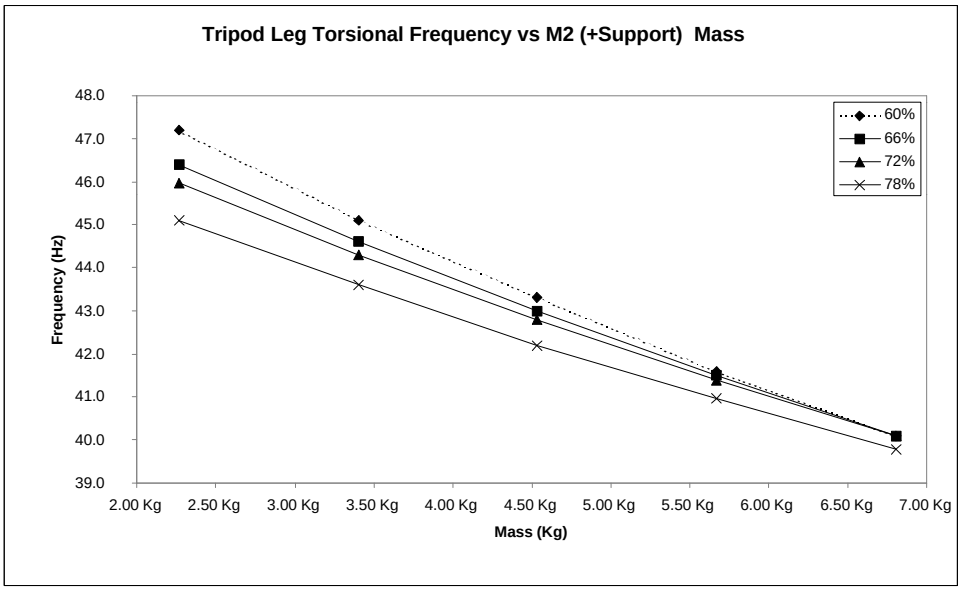

FIGURE 5.7 Torsional Frequency Sensitivity to Supported mass and Constraint Location

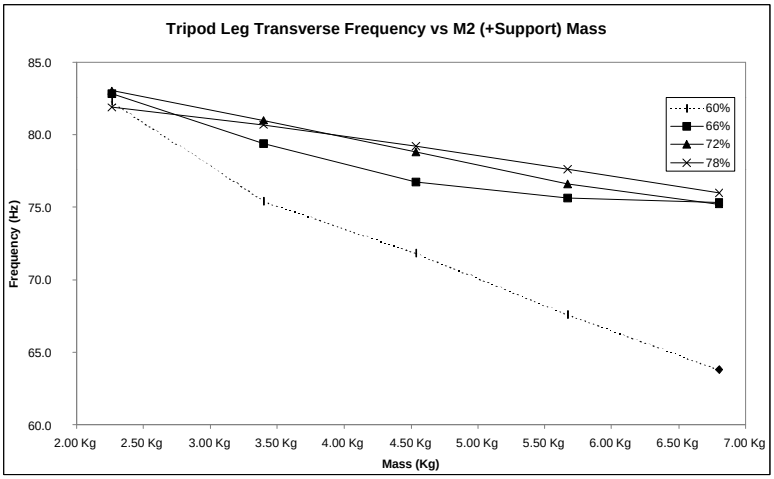

FIGURE 5.8 Transverse Frequency Sensitivity to Supported mass and Constraint Location

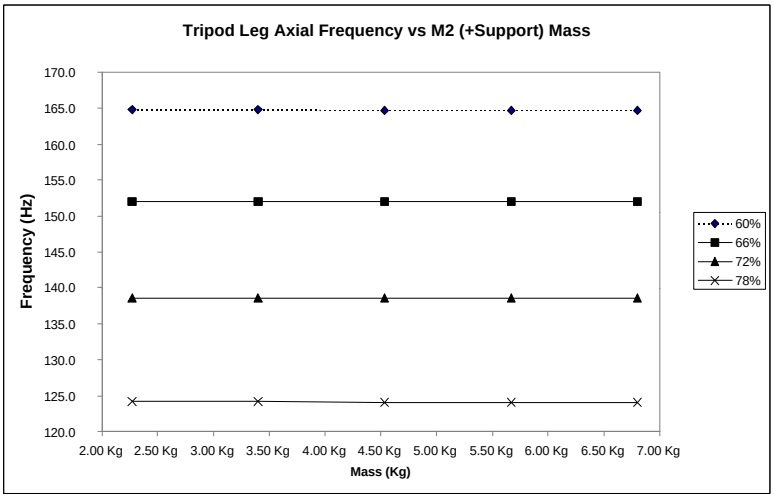

FIGURE 5.9 Axial Frequency Sensitivity to Supported mass and Constraint Location

While the axial frequency is insensitive to the change in supported mass over the ranges considered, increasing the supported mass decreases the torsional and transverse frequencies. Increasing the constraint location decreases the torsional and axial frequency, but increases the transverse frequency. As can be seen from the figures, the sensitivities of the dynamic results are such that meeting the frequency requirements is feasible, and the requirements can be easily met with ample margin, even though the analysis models do not yet contain the required fidelity for a detailed analysis.

5.2.1.3 Sensitivity to Modeling Assumptions

The results obtained in the analysis depend strongly on the assumptions used in the modeling of the structure. The frequency results can be expected to drop when accounting for the flexibility of the secondary mirror support structure, connections to

tripod legs, and the flexures. However, the smallest current margin on the eigenfrequencies is of forty percent, for the torsional frequency. This is sufficient margin to account for the modeling assumptions used in the analysis. Therefore, it is expected that the frequency requirements will be easily met, even when including details of the structural components which have not been accounted in the finite element models and in the analysis.

Operational Analysis (To Be Done (TBD))

5.3.1 Response to Residual Inertial Loads and Stresses (TBD)

5.3.2 Response to Residual Moisture Perturbations (TBD)

5.3.3 Response to Thermal Perturbations (TBD)

5.4 Test Analysis

The FIRST Telescope, under the verification plan, will be tested in a thermal-vacuum environmental chamber. Since such testing will occur under earth's gravity, the telescope design must consider the performance of the telescope assembly under testing conditions, as well as operating conditions. Thus, the design is dependent on specifics of test chamber selection, earth's gravity field magnitude and orientation, the fixturing scheme, and the chamber boundary conditions. The testing configuration, testing strategy, and gravity release mechanism (if any) dictate the amount of decenter, defocus, and tilt of the secondary mirror relative to the primary mirror, as well as distortions in the primary mirror, and primary mirror mount. In Section 3, Telescope Optical Design, the sensitivity of the Telescope root mean square wavefront error to each of these perturbations is described.

Based on these and other considerations, the current strategy for testing the telescope is to align the optical axis to coincide with earth's gravity. When the optical axis of the telescope is aligned with earth's gravity, the expected defocus is more manageable than the expected amount of tilt and decenter expected if the telescope assembly were tested with its optical axis transverse to the gravity field. Horizontal testing would imply stiffer struts with an increase in the associated obscuration, emission and mass penalties, and is therefore not planned for the final tests, nor is such testing a design parameter.

5.4.1 Perturbations due to 1-g

The telescope assembly will experience deflections during testing due to the earth's gravity field. The choice and availability of test chambers will determine the type of perturbations which need to be accounted for during testing and data correlation. If the telescope's optical axis is in the direction of gravity, the amount of defocus needs to remain at acceptable levels to ensure that testing can be performed successfully. If the telescope's optical axis is perpendicular to the gravity field, then the secondary mirror's decenter and tilt become more important parameters to consider.

The magnitude of the deflections due to earth's gravity were predicted by using the same finite element models used to compute the fundamental vibration frequencies, but with the primary mirror omitted from the finite element model. In addition, different boundary conditions were utilized for these cases. Rather than assuming a kinematic mount (constrained in optical axis direction and in tangential direction only) at the locations where the tripod legs connect to the primary mirror, the locations were assumed to be pinned (constrained from translating in all directions, but free to rotate in any direction). By using these boundary conditions, the predicted deformations account only for the flexibility of the tripod legs. The boundary conditions do not account for the flexibility

of the primary mirror and flexures; their contributions being accounted for independently. If the boundary conditions in this analysis were assumed to be those of an ideal kinematic mount, then the perturbations at the secondary mirror would be the superposition of the deformations. Deformations are due to the tripod legs' innate flexibility, plus the translation and rotation of the secondary mirror due to any translation of the legs at their base and in the radial direction.

In order to illustrate the superposition of the two effects, the following two figures are shown. Figure 5.10 shows the deflection of the tripod legs assuming that the tripod leg bases are mounted simulating a kinematic mount (constrained in optical axis direction and in tangential direction only). The position of the secondary mirror relative to the primary mirror depends on the stiffness of the tripod legs, as well as on the amount of translation in the radial direction experienced by the tripod leg bases. The amount of radial translation of the tripod leg bases in turn depend on the in-plane stiffness of the primary mirror, flexure design, and mounting scheme. In order to isolate the effects which can be attributed to the tripod leg flexibility from the other components, the tripod leg bases were assumed to be pinned in the analysis (constrained from translating in all directions, but free to rotate in any direction). The deflection of the tripod legs under these conditions is shown in Figure 5.11.

When the optical axis is perpendicular to the gravity field, the deflection effects due to the ability of the tripod legs to translate are small relative to the deflection of the tripod legs. When the optical axis is aligned with the gravity field, the deflection effects due to the ability of the tripod legs to translate are of the same order as the deflection attributable to the tripod leg flexibility.

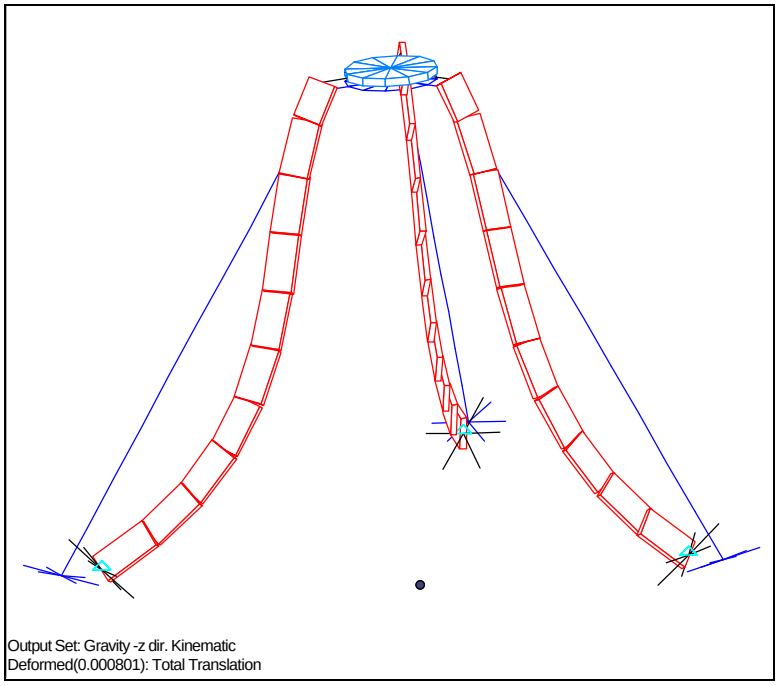

Figure (5.10) Exaggerated deflection of tripod legs assuming bases can translate in radial direction (due to primary mirror sag, pulling the tripod legs

toward optical axis. M2 may actually move away from M1 due to legs change in "effective" angle)

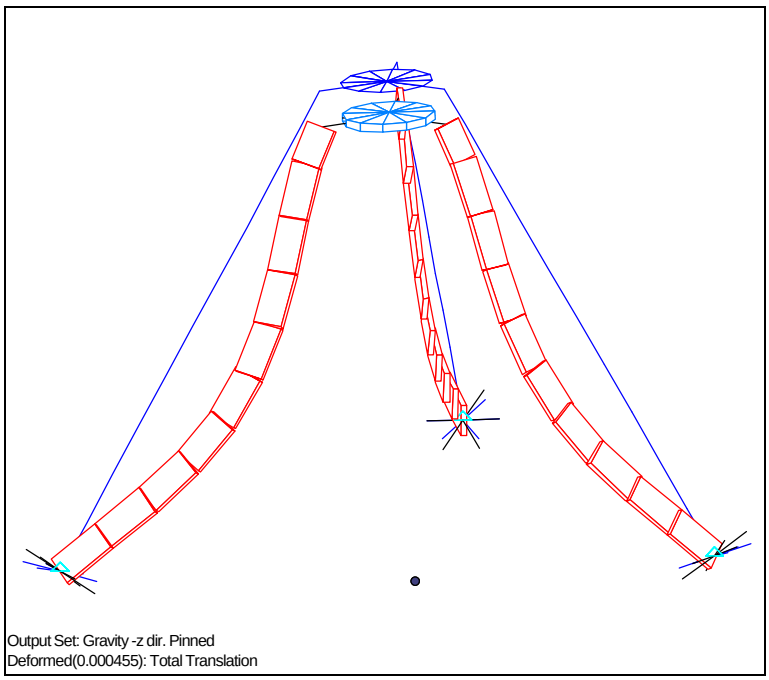

Figure (5.11) Exaggerated deflection of tripod legs assuming base of tripod legs cannot translate in radial direction

5.4.1.1 Perturbations due to 1-g in Direction Transverse to Optical Axis

Based on the tripod leg configuration described previously, the expected amount of decenter and tilt of the secondary mirror due to gravity acting in the transverse direction was predicted analytically. Figure 5.12 shows the magnitude of M2 decenter as a function of the mass supported by the tripod legs, for various tripod leg constraint locations. Similarly, Figure 5.13 shows the amount of tilt expected at M2.

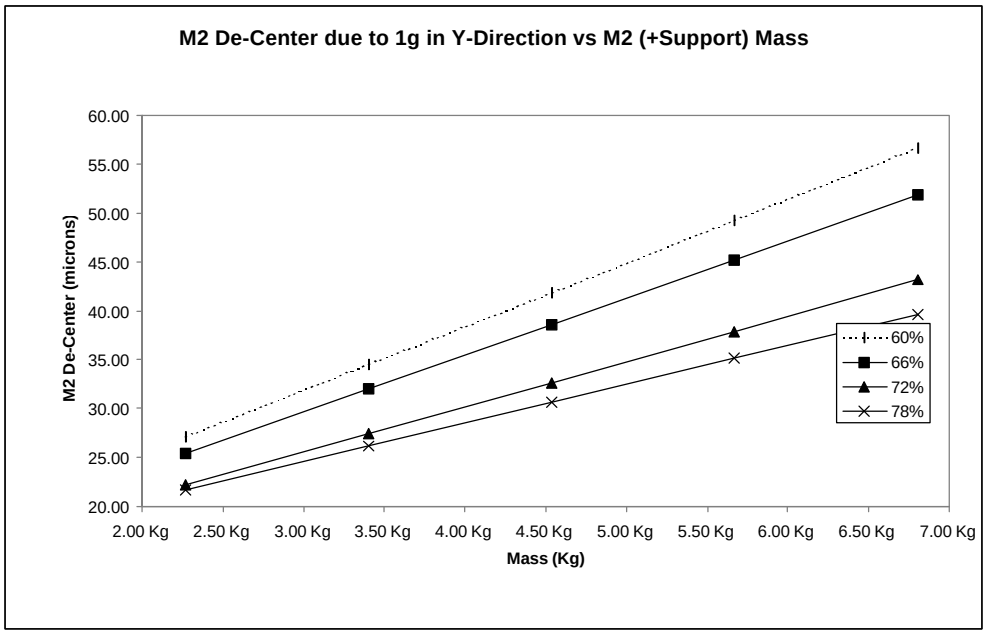

FIGURE 5.12 M2 De-Center due to 1g in Transverse Direction

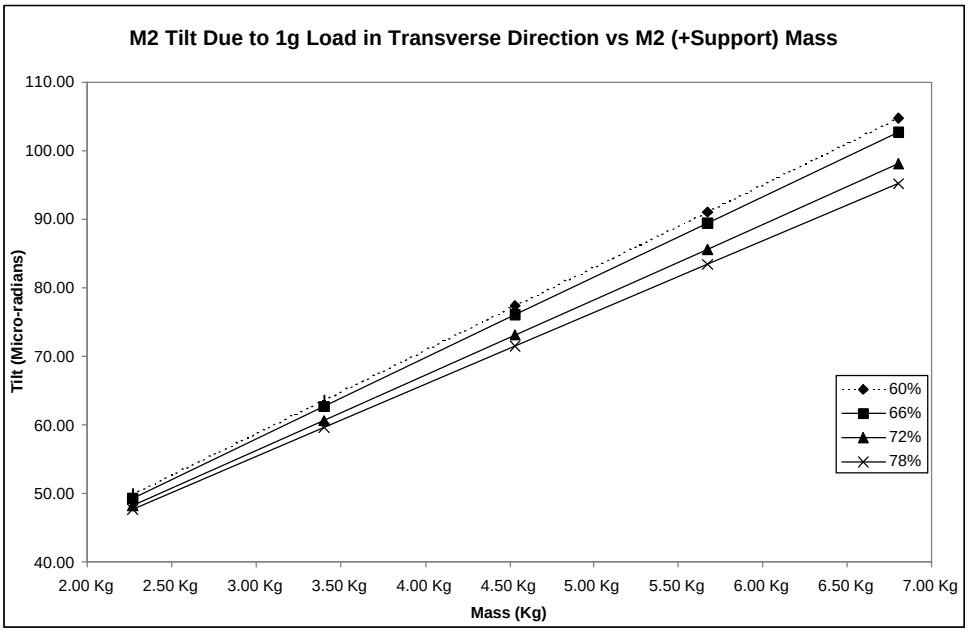

FIGURE 5.13 M2 Tilt due to 1g in Transverse Direction

Tables 5.5 and 5.6 summarize the results for the various configurations considered.

De-center due to gravity in transverse direction (micrometers)				
	60%	66%	72%	78%
2.27 kg	27.11	25.40	22.21	21.68
3.40 kg	34.49	32.00	27.45	26.18
4.54 kg	41.86	38.61	32.68	30.68
5.67 kg	49.24	45.21	37.91	35.18
6.80 kg	56.61	51.81	43.14	39.68

TABLE 5.5 Secondary mirror decenter due to gravity acting in transverse direction for various masses supported by the tripod legs and for various constraint locations

Tilt due to gravity in transverse direction (microradians)				
	60%	66%	72%	78%
2.27 kg	49.86	49.30	48.18	47.69
3.40 kg	63.57	62.65	60.66	59.56
4.54 kg	77.28	76.00	73.14	71.44
5.67 kg	90.99	89.35	85.62	83.32
6.80 kg	104.71	102.70	98.10	95.19

TABLE 5.6 Secondary mirror tilt due to gravity acting in transverse direction for various masses supported by the tripod legs and for various constraint locations

The analysis predicts a decenter in the range of 30 to 40 micrometers attributable to the tripod legs when supporting 4.5 kg. The amount of tilt predicted for the same conditions is in the order of 70-80 microradians.

5.4.1.2 Perturbations due to 1-g in Optical Axis Direction

The amount of defocus expected due to gravity acting in the direction of the optical axis was predicted analytically. Figure 5.14 shows the amount of defocus as a function of the mass supported by the tripod legs, for various tripod leg constraint locations. The results are summarized in Table 5.7.

De-focus due to gravity in optical axis direction (micrometers)		
	60%	72%
2.27 kg	0.58	0.71
3.40 kg	0.78	0.94
4.54 kg	0.97	1.17
5.67 kg	1.17	1.40
6.80 kg	1.36	1.63

TABLE 5.7 Secondary mirror defocus due to gravity acting in transverse direction for various masses supported by the tripod legs and for various constraint locations

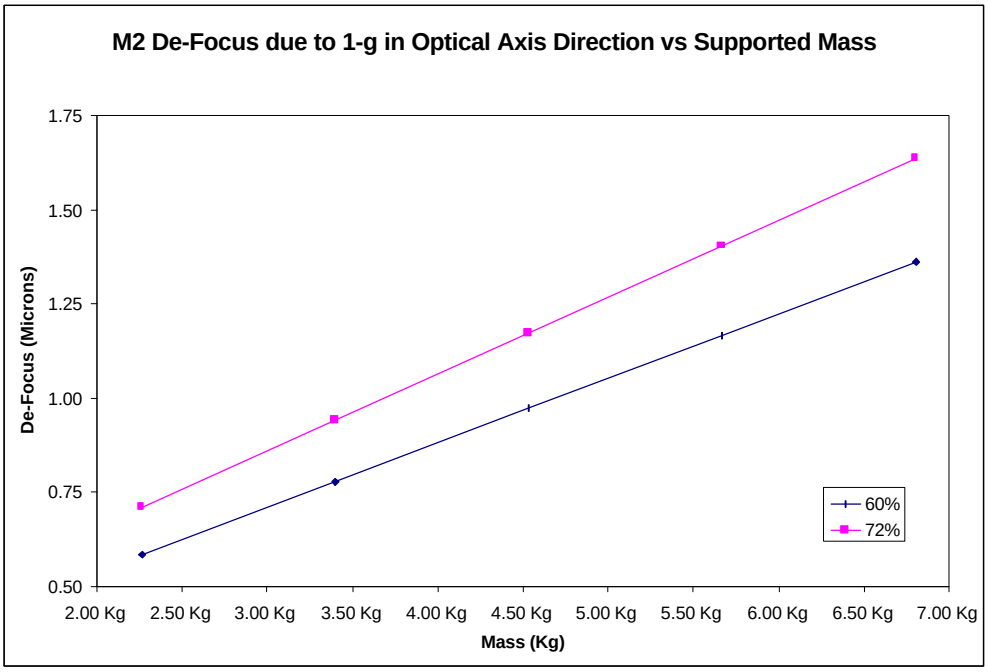

FIGURE 5.14 M2 De-Focus due to 1-g in Optical Axis Direction

The analysis predicts a defocus of less than two micrometers attributable to the tripod leg flexibility when supporting any of the masses considered.

Although the current tripod leg configuration is expected to satisfy the specification requirements based on the results of this report, it is not clear yet whether or not it meets the internal requirements which are necessary for successfully testing the telescope assembly in an environmental chamber under earth's gravity. These considerations are currently being investigated, and may require some modifications to the tripod design.